Water Science & Technology

IWA PUBLISHING

Water Science & Technology Vol 85 No 6, 1813 doi: 10.2166/wst.2022.073

Heterogeneous activation of $H_2O_2/Na_2S_2O_8$ with iron ore from water distribution networks for pollutant removal

Dan Zhong[a,†], Fu He[a,†], Wencheng Ma[a,*], Yichuan Wu[a] and Jiaju Dong[b]

[a] School of Environment, Harbin Institute of Technology, Harbin 150090, P.R. China
[b] Shenzhen New Land Tool Planning & Architectural Design Co., Ltd., P.R. China
*Corresponding author. E-mail: damahit@163.com
†These authors contributed equally to this paper.

WM, 0000-0003-1167-5292

ABSTRACT

In this study, we investigated using the main composition of pipe deposits from water distribution networks as catalyst to activate dual-oxidant $H_2O_2/Na_2S_2O_8$ system to produce radicals for perchloroethylene and chloramphenicol removal. According to the results, the degradation efficiency of perchloroethylene by $H_2O_2/Na_2S_2O_8$ system was 92.05% within 8 h. Due to the slow conversion between $\equiv Fe^{3+}$ and $\equiv Fe^{2+}$, the hydroxylamine was introduced to reduce reaction time. As for the results, the degradation efficiency of chloramphenicol in the $H_2O_2/Na_2S_2O_8$ system with hydroxylamine assistance was 73.31% within 100 min. Meanwhile, several key affecting factors and the kinetic models were investigated. The primary radicals were identified by electron paramagnetic resonance and radical scavenging tests. Eleven degradation products were confirmed by high-resolution liquid chromatography-mass spectrometry. The result of this study provided the theoretical basis for resource utilization of pipe deposits in water treatment in case of emerging contamination events.

Key words: γ-FeOOH, chloramphenicol, dual-oxidant, hydroxyl radical, synergistic effect

1. INTRODUCTION

Perchloroethylene (PCE) is an important organic solvent, which is widely used in the cleaning industry of machinery, electronic parts and clothing, as well as in the production of medicine, textiles, and chemicals (Zhong *et al.* 2019). Chloramphenicol (CAP) is a bacteriostatic broad-spectrum antibiotic, which is widely used in disease treatment, animal husbandry and aquaculture (Cao *et al.* 2020). PCE and CAP have been detected in surface water, ground water and even drinking water because of the unreasonable usage and disposition. PCE and CAP can cause various diseases including leukemia, kidney and liver tumors (Zhong *et al.* 2019), bone marrow depression and aplastic anemia (He *et al.* 2020) which are serious and widespread problems (Shapiro *et al.* 2004; Walters *et al.* 2010).

Various remediation technologies were used to remove PCE and CAP from water. It is well-known that the advanced oxidation processes (AOPs) based on hydroxyl radicals (•OH) and sulfate radicals ($SO_4^{\bullet-}$) are considered as effective methods to mineralize organic pollutants (Wu *et al.* 2018). Hydrogen peroxide (H_2O_2, HP), peroxymonosulfate($KHSO_5{\cdot}0.5KHSO_4{\cdot}0.5K_2SO_4$, PMS) and persulfate($Na_2S_2O_8$, PS) are the common oxidants to produce radicals for degrading pollutants (Luo *et al.* 2021a). The •OH-AOPs and $SO_4^{\bullet-}$-AOPs have their respective advantages. The •OH-AOPs have a high reaction rate and are nonselective for organics, $SO_4^{\bullet-}$-AOPs are stable and selective and $SO_4^{\bullet-}$ has a longer half-life time than •OH. However, in order to achieve the same efficiency, the PS or PMS dosage must be very high which leads to higher salinity in the system (Gu *et al.* 2019). The dual-oxidant system could reduce oxidant usage and utilize their respective advantages in removal pollutants and have faster degradation rate (Chen *et al.* 2020; He *et al.* 2020; Song *et al.* 2020). The combined application of HP and PS to generate •OH and $SO_4^{\bullet-}$ has been studied to treat various pollutants including levofloxacin (Epold *et al.* 2015), erythromycin (Li *et al.* 2017), trichloroethylene (Yan *et al.* 2013), 2,4-dinitrotoluene (Xu *et al.* 2019), and even industrial wastewater (Chen *et al.* 2020).

Iron-containing materials are the most commonly used catalysts to activate HP, PS and PMS because of its cost-effectiveness and eco-friendliness (Rastogi *et al.* 2009; Romero *et al.* 2010). Some researchers found that the pipe deposits are iron-rich

including α-FeOOH, γ-FeOOH, γ-Fe_2O_3 and Fe_3O_4, etc. (Oliveira *et al.* 2012; Cui *et al.* 2016). The pipe deposits could be used as inexpensive catalysts in heterogeneous Fenton-like oxidation, which attracted increasing attention (Oliveira *et al.* 2012). In our previous study, we explored the adsorption and degradation capacity of simulated pipe deposits (SGR, the mixture of the major constituents of actual pipe deposits (α- and γ-FeOOH)) for 5-bromosalicylic acid(5-BSA), 32.65% and 87.67% of 5-BSA could be removed by adsorption and SGR/H_2O_2 oxidation (Huang *et al.* 2021). The findings of previous study would make an important contribution to pipe deposits recycling. However, the removal time was too long, and the mechanisms and kinetics were not discussed in detail.

In this study, we analyzed and prepared the main composition of pipe deposits, γ-FeOOH, which is used as a catalyst to activate HP/PS in order to produce radicals for PCE and CAP removal. The hydroxylamine (NH_2OH, HA) was introduced to increase the degradation rate and shorten the degradation time. Furthermore, the underlying mechanism was investigated by radical scavenging test (RST), electron paramagnetic resonance (EPR) and X-ray photoelectron spectroscopy (XPS). The method may be expected to be used for *in situ* treatment of polluted water of the network emergency contamination.

2. MATERIALS AND METHODS

2.1. Materials

PCE was obtained from Tianjin Bodi Chemicals Co., Ltd $FeCl_2{\cdot}4H_2O$ and NaOH were purchased from Sinopharm Chemical Reagent Co., Ltd CAP, H_2O_2, $Na_2S_2O_8$, NH_2OH, para-chlorobenzoic acid (pCBA) and 5,5-Dimethyl-1-pyrroline-N-oxide (DMPO) were obtained from Shanghai Aladdin Biochemical Technology Co., Ltd. Methanol(MeOH), tert-butanol(TBA) and isopropanol were from Tianjin Guangfu Fine Chemical Research Institute. All the chemicals were used without any further purification. All solutions were prepared by deionized water.

2.2. Preparation of lepidocrocite

Lepidocrocite (γ-FeOOH) was synthesized at 25 °C. Firstly, 4 g $FeCl_2{\cdot}4H_2O$ were added to 100 mL deionized water and continuously stirred, and maintained the solution pH at 6.8 $\pm$ 0.1 by adding 1.0 mol L^{-1} NaOH. Then, air (36 – 72 L h^{-1}) was sent into the solution and maintained pH at 6.8 $\pm$ 0.1 until the color of suspension changed from dark green to orange. Finally, the prepared γ-FeOOH was centrifuged and washed with deionized water and dried (Antony *et al.* 2005).

2.3. PCE and CAP removal and detection

All batch removal experiments were conducted in a 100 mL capped bottle at 25 °C. A certain number γ-FeOOH were added to 100 mL aqueous solution containing PCE or CAP. HA, HP and PS were added to the abovementioned solution at appropriate concentration to perform degradation experiments. 0.1 mol L^{-1} HCl and 0.1 mol L^{-1} NaOH was used to adjust the pH of pollutant solution. The PCE was extracted by n-hexane and the residual concentration was detected by GC-ECD. The CAP residual concentration was detected by a UV-vis spectrophotometer at 277.6 nm. The detected peak did not shift which indicated that the addition of reagents did not influence CAP detection, as shown in Fig. S1. All experiments were conducted in triplicate.

2.4. Confirmed the rate constant of the pollutant with radicals

The rate constant of CAP with radicals ($k_{\cdot OH,CAP}$) was studied by competition kinetics method (Cao *et al.* 2020). pCBA ($k_{\cdot OH,\ pCBA} = 5.00 \times 10^9\ M^{-1}s^{-1}$) was used for the competitor. The adsorption of CAP and pCBA by γ-FeOOH and photodegradation were negligible. The rate constant of CAP with •OH could be estimated by the following equation:

$$ln\left\{\frac{pCBA_0}{pCBA_t}\right\}/k_{\cdot OH,\ pCBA} = ln\left\{\frac{CAP_0}{CAP_t}\right\}/k_{\cdot OH,CAP} \quad (1)$$

Rearranging Equation (1) got Equation (2)

$$k_{\cdot OH,CAP} = k_{\cdot OH,pCBA} \times ln\left\{\frac{CAP_0}{CAP_t}\right\}/ln\left\{\frac{pCBA_0}{pCBA_t}\right\} \quad (2)$$

$k_{\cdot OH,pCBA}$ was the reaction rate constant of •OH with pCBA.
$k_{\cdot OH,CAP}$ was the reaction rate constant of •OH with CAP.

2.5. Characterization

Scanning electron microscope (SEM, ZEISS Sigma 500, Instrument Parameter: EHT = 15.00 kV, Signal A = SE2, WD = 8.4 mm, Mag = 20.00 KX) was used to observe the morphology of γ-FeOOH. X-ray diffraction with 2θ range from 10 to 90° was used to analyzed the crystalline structure of γ-FeOOH(XRD, AXS D8 ADVANCE with CoKα radiation (λ = 1.54060 Å)). X-ray photoelectron spectroscopy (XPS, AXIS ULTRA DLD using Al Ka radiation (1,486.6 eV)) were used to explore the surface valence state of γ-FeOOH before and after degradation. The chemical groups on γ-FeOOH surface were detected by Fourier transformation infrared spectroscopy (FTIR, Perkin Elmer Spectrum One). The main radicals were detected by electron paramagnetic resonance (EPR, Bruker, Germany) with DMPO as the spin-trapping agent. The degradation products were determined by high-resolution LC-MS in negative ionization mode using an Agilent 1260 HPLC coupled with ABSciexQTrap 5500 MS with an electrospray ionization (ESI) source. The MS instrumental parameters were set as follows: source temperature, 500 °C; Gas I, 50 arbitrary units; Gas II, 50 arbitrary units; negative ion spray voltage, 4500 V; curtain gas, 50 arbitrary units; entrance potential (EP), 10 V; declustering potential (DP), 100 V; collision energy (CE), 30 V; collision cell exit potential (CXP), 20 V; PIS scan range, 100–1000 amu.

3. RESULTS AND DISCUSSIONS

3.1. Morphology and structural characterization of γ-FeOOH

γ-FeOOH was a rod-type structure by the SEM observation (Figure 1(a)). The XRD patterns (Figure 1(b)) showed that the diffraction peaks at 2θ = 14.16°, 27.16°, 36.14° and 46.89° were attributed to (200), (210), (301) and (501) lattice planes of

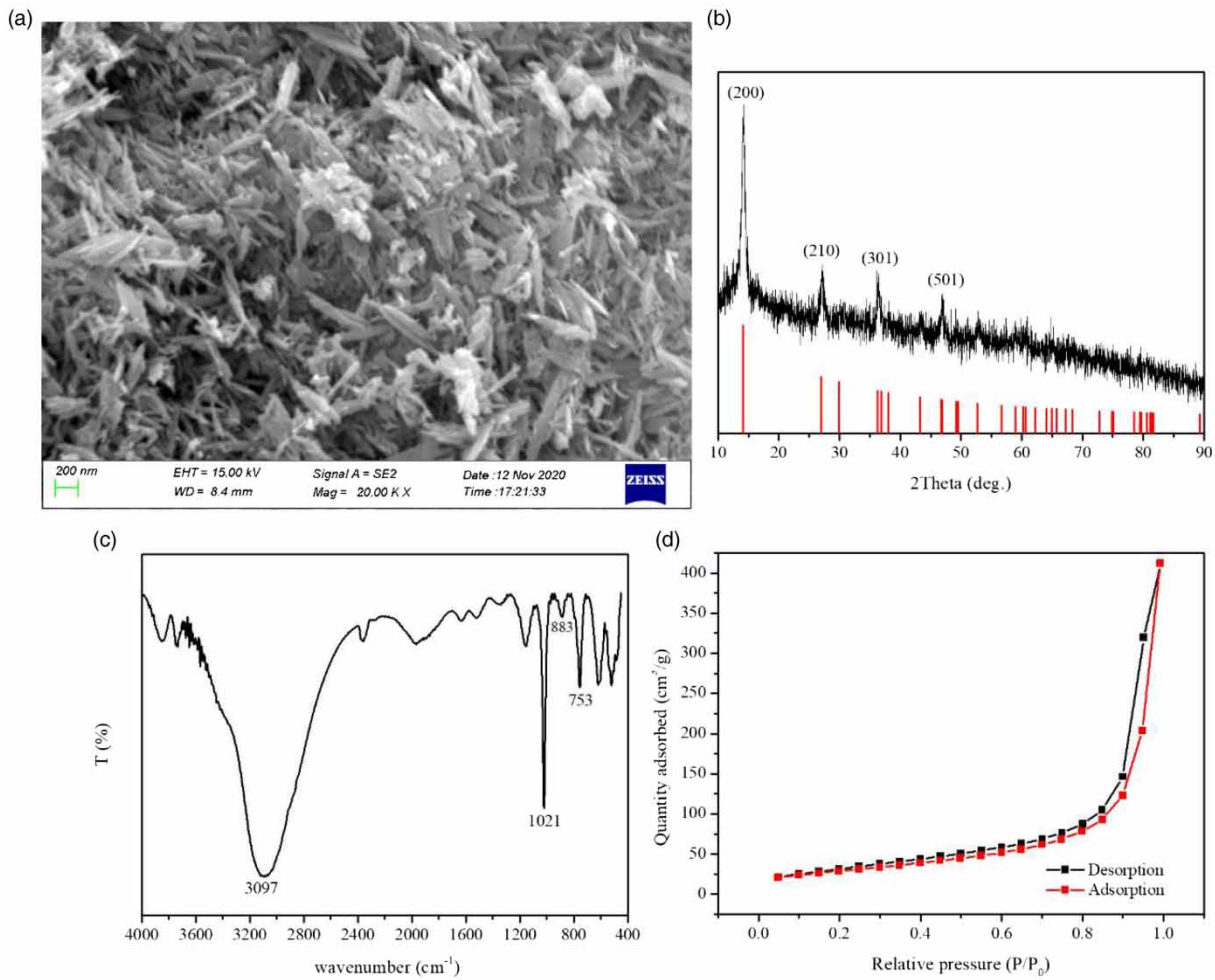

Figure 1 | Characterizations of the prepared γ-FeOOH: (a) SEM image, (b) XRD spectrum, (c) FTIR spectrum and (d) N_2 adsorption-desorption curve.

Lepidocrocite, syn (JCPDS No. 44-1415) (Shao *et al.* 2022). The stronger intensity and narrower half peak width suggested that γ-FeOOH was a consistent crystal structure. According to the FTIR spectrum (Figure 1(c)), the peak appeared at 1021 cm^{-1} was the in-plane of Fe-O-H bending vibrations, while the peak appeared at 753 cm^{-1} was for the out-plane (He *et al.* 2018). These results verified the successful preparation of γ-FeOOH. Figure 1(d) showed that the N_2 adsorption-desorption isotherms of the prepared γ-FeOOH is type IV with H3 hysteresis loop, demonstrating its microporous/mesoporous structure (Li *et al.* 2019; Liu *et al.* 2019). Meanwhile, γ-FeOOH has a rather larger specific surface area (117.567 m^2/g), average pore size (23.8672 nm) and pore volume (0.6382 cm^3/g). The larger specific surface area could expose more active sites, which was conducive to increasing reaction activity (Lyu *et al.* 2021).

3.2. The degradation PCE and CAP in different systems

The PCE degradation under different systems was explored, the result was showed in Figure 2(a). Due to the volatilization and adsorption, 15.33% PCE was removed. 92.05% PCE was removed in HP/PS system in 8 h. The PCE degradation efficiency in dual-oxidant system was higher than in the single-oxidant system, HP/PS > HP > PS. The removal of CAP in γ-FeOOH, γ-FeOOH/HP/PS, γ-FeOOH/HA/HP, γ-FeOOH/HA/PS and γ-FeOOH/HA/HP/PS was shown in Figure 2(b). When γ-FeOOH was added alone, CAP was not removed indicating that γ-FeOOH had no adsorption. In addition, CAP could not be degraded effectively by γ-FeOOH/HP/PS system, indicating that γ-FeOOH cannot activate HP and PS to produce radicals. When the HA was introduced into the system and the usage of oxidant was the same, the degradation efficiency of CAP in γ-FeOOH/HA/HP, γ-FeOOH/HA/PS and γ-FeOOH/HA/HP/PS system was 63.18%, 14.11% and 73.31% in 100 min, respectively. And the CAP degradation in HP/PS, HP and PS system could be well fitted by the first-order kinetics model as expressed by Equation (3) (Zhou *et al.* 2014), the detail fitting results of CAP were shown in Figure 2(c) and Table 1.

$$\frac{lnC_0}{lnC_t} = kt \tag{3}$$

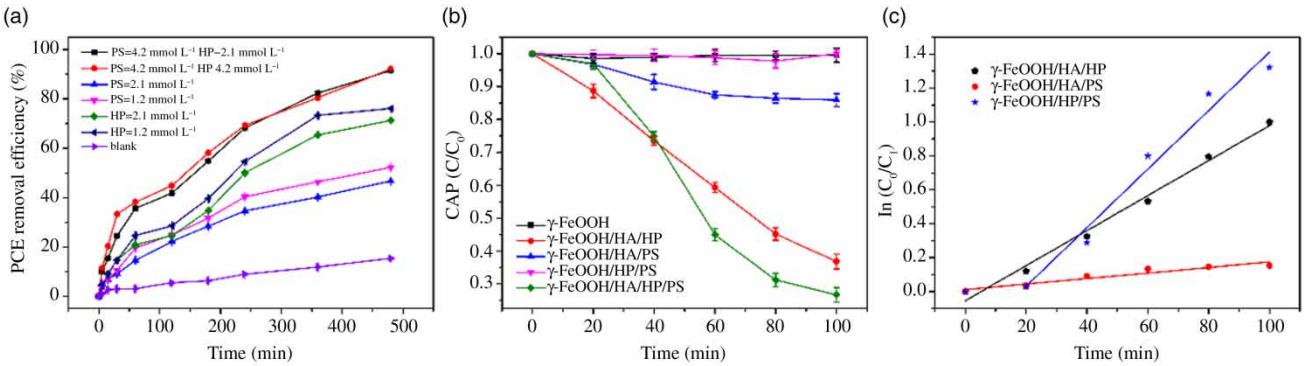

Figure 2 | The (a) PCE and (b) CAP degradation under different systems; (c) The kinetic fitting curve of CAP under different systems. Reaction conditions: (a) $[PCE]_0 = 163$ mg L^{-1}, $[\gamma\text{-FeOOH}]_0 = 22.5$ mmol L^{-1}; (b) $[CAP]_0 = 20$ mg L^{-1}, $[\gamma\text{-FeOOH}]_0 = 5.6$ mmol L^{-1}, $[HA]_0 = 2$ mmol L^{-1}, (Oxidants: $[HP]_0 = [PS]_0 = 4$ mmol L^{-1} in γ-FeOOH/HA/HP and γ-FeOOH/HA/PS system, respectively; $[HP]_0 = [PS]_0 = 2$ mmol L^{-1} in γ-FeOOH/HA/HP/PS system), pH = 6.5, T = 25 °C.

Table 1 | The kinetic parameters of CAP degradation in different systems and the oxidant decomposition kinetic parameters

System	k(min^{-1})	R^2
γ-FeOOH/HA/HP	0.0103	0.9904
γ-FeOOH/HA/PS	0.0023	0.9911
γ-FeOOH/HA/HP/PS	0.0173	0.9740
HP decomposition (Figure 4(b))	0.0139	0.9917
PS decomposition (Figure 4(c))	0.0076	0.9967
	0.0024	0.9980

k is the kinetic rate constant, which can be calculated from the slope of the straight line.

The rate constant of γ-FeOOH/HA/HP/PS system was 0.0173 min^{-1}, which was higher than γ-FeOOH/HA/HP(0.0103 min^{-1}) and γ-FeOOH/HA/PS (0.0023 min^{-1}). The results indicated that the HP/PS system has the unique advantages in pollutant removal because of synergistic effect.

3.3. Effect of experimental conditions

AOPs are complicated systems, and many factors could influence their performance. In order to better clarify the mechanism of dual-oxidant system, the detailed effect of different experimental conditions on CAP degradation were studied.

3.3.1. Effect of the initial pH

The initial pH is a significant role in the AOPs. In the γ-FeOOH/HA/HP/PS system, the initial pH of the solution was adjusted by using sodium hydroxide or hydrochloric acid and no buffering agents were introduced. As shown in Figure 3(a), the degradation efficiency was over 75% when the pH ranged from 3.0 to 9.0. However, the degradation was obviously inhibited at pH = 11. The variation of solution H^+ concentration was monitored (Figure 3(b)). The eventual pH all dropped to acidic, as shown in Table 2. The acidic conditions favored the reaction between γ-FeOOH and oxidant to produce radicals for target pollutant removal. According to the previous studies, if the eventual pH was higher than 4, the iron precipitation formed on the surface of γ-FeOOH that lead to a passivation phenomenon, which was harmful for the CAP degradation. The eventual pH was 6.35 when the initial was pH = 11, the CAP degradation was suppressed. Our results were consistent with previous studies (Rao *et al.* 2014). The increased H^+ was because of the reaction between $SO_4^{\bullet -}$ and H_2O to form •OH via one-electron transfer process, as shown in Equation (4). These results demonstrated that the HP/PS dual-oxidant process can remove CAP in acidic and slightly alkaline.

$$SO_4^{\bullet -} + H_2O \rightarrow SO_4^{2-} + \bullet OH + H^+ \quad (4)$$

3.3.2. Effect of the initial HP or PS concentration

HP and PS are the main source of radicals. It is important to optimize the dose of oxidants for the effective degradation of organic pollutants. Figure 3(c) and 3(d) described the effect of HP and PS concentration on CAP degradation. The increase of initial HP and PS concentration resulted in a noticeable enhancement in CAP degradation, which was because of there being the enough radicals. According to the experimental results, 2 mmol L^{-1} PS and 4 mmol L^{-1} HP was the optimum dosage, the CAP degradation efficiency could reach to 78.43% in 100 min. However, when the HP or PS concentration were further increased, the degradation efficiency decreased. The excessive HP and PS might result in the scavenge of •OH and $SO_4^{\bullet -}$ into the lower oxidizing ability species, which led to the low degradation efficiency. The detail process was shown in Equations (5)–(8) (Cai *et al.* 2016; Gao *et al.* 2022).

$$\bullet OH + H_2O_2 \rightarrow HO_2\bullet + H_2O \quad (5)$$

$$\bullet OH + HO_2\bullet \rightarrow H_2O + O_2 \quad (6)$$

$$SO_4^{\bullet -} + S_2O_8^{2-} \rightarrow S_2O_8^{\bullet -} + SO_4^{2-} \quad (7)$$

$$SO_4^{\bullet -} + SO_4^{\bullet -} \rightarrow S_2O_8^{2-} \quad (8)$$

3.3.3. Effect of the iron ore dosage

The influence of the iron ore dosage on CAP degradation was investigated using the catalyst from 1.4 mmol L^{-1} to 11.2 mmol L^{-1}, as shown in Figure 3(f). The increase of catalyst dosage provided more active sites for the reaction of HP/PS with antibiotics, resulting in high degradation rate. In contrast to our previous studies about the goethite activating HP/PS system (He *et al.* 2020), the lepidocrocite system did not have an induction period because the lepidocrocite has a larger specific surface area than goethite, which causes more $\equiv Fe^{3+}$ to be reduced and to accumulate more radicals with the catalyst dosage at the same time.

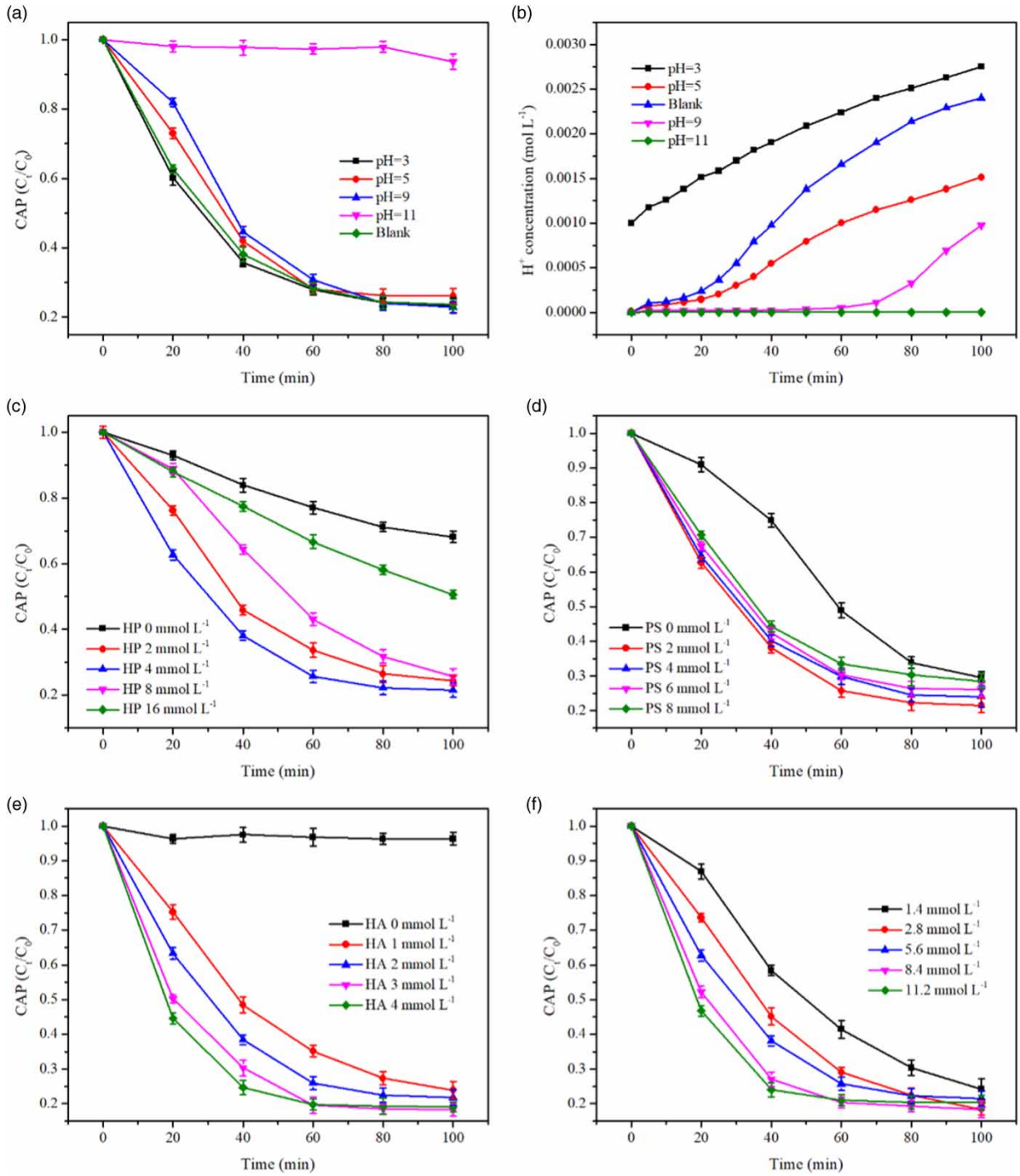

Figure 3 | Effect of (a) the initial pH; (b) the H^+ concentration variation at different initial pH; Effect of (c) the HP concentration, (d) the PS concentration; (e) the HA concentration and (f) the catalyst dosage on CAP degradation. (Reaction conditions: (a) $[CAP]_0 = 20$ mg L^{-1}, $[\gamma\text{-FeOOH}]_0 = 5.6$ mmol L^{-1}, $[HA]_0 = [PS]_0 = 2$ mmol L^{-1}, $[HP]_0 = 4$ mmol L^{-1}, T = 25 °C; (c) $[CAP]_0 = 20$ mg L^{-1}, $[\gamma\text{-FeOOH}]_0 = 5.6$ mmol L^{-1}, $[HA]_0 = [PS]_0 = 2$ mmol L^{-1}, T = 25 °C; (d) $[CAP]_0 = 20$ mg L^{-1}, $[\gamma\text{-FeOOH}]_0 = 5.6$ mmol L^{-1}, $[HA]_0 = 2$ mmol L^{-1}, $[HP]_0 = 4$ mmol L^{-1}, T = 25 °C; (e) $[CAP]_0 = 20$ mg L^{-1}, $[\gamma\text{-FeOOH}]_0 = 5.6$ mmol L^{-1}, $[HP]_0 = 4$ mmol L^{-1}, $[PS]_0 = 2$ mmol L^{-1}, T = 25 °C; (f) $[CAP]_0 = 20$ mg L^{-1}, $[HA]_0 = [PS]_0 = 2$ mmol L^{-1}, $[HP]_0 = 4$ mmol L^{-1}, T = 25 °C.).

3.4. The residual HP and PS concentration and the kinetics fitting curves

The Figure 4(a) exhibited the residual HP and PS concentration in γ-FeOOH/HA/HP/PS system. After 100 min, the consumption of HP and PS was 75.37% and 42.81%, and the decomposition of PS was two-stage reaction. The Figure 4(b)

Table 2 | The pH of before and after degradation

	The initial pH	The final pH
γ-FeOOH/HA/HP/PS	3	2.56
	5	2.82
	9	3.01
	11	6.35
	Blank (6.5)	2.62

and 4(c) were the kinetics fitting curves of HP and PS decomposition in γ-FeOOH/HA/HP/PS system, respectively. The detail kinetic parameters were shown in Table 1. HP decomposition was fitted well by the first-order kinetics model and the rate constant was 0.0139 min^{-1}. PS decomposition was a two-phase reaction. In the initial phase (0–60 min), the rate constant was 0.0076 min^{-1}. In the second phase (60–100 min), the rate constant was 0.0024 min^{-1}. At the beginning of the reaction, PS was rapidly decomposed due to the accumulation of a large amount of $\equiv Fe^{2+}$ by HA reduction. The HA was consumed which led to the slow conversion of $\equiv Fe^{3+}$ to $\equiv Fe^{2+}$. Therefore, the PS decomposition entered a slow process.

3.5. The confirmation of active species and reaction rate constants

In order to confirm the primary radicals in CAP degradation by γ-FeOOH/HA/HP/PS system, DMPO was used as a trapping agent to conduct the EPR test. DMPO can react with radicals to generate adducts, such as DMPO-OH and DMPO-SO_4. The strong EPR signal (shown in the Figure 5(a)) was DMPO-OH, simultaneously, the low peaks were most likely to be DMPO-SO_4. PS may be first activated by γ-FeOOH to produce $SO_4^{\bullet-}$ and then react with the adsorbed water to lead to the production of abundant •OH via one-electron transfer process, which was consistent with the H^+ increase. The similar phenomenon has reported in previous studies (Huang *et al.* 2014; Duan *et al.* 2016).

Methanol (MeOH), tert-butanol (TBA) and isopropanol were used as quenchers to perform the quenching tests (Figure 5(b)). The reaction rate constants were $k_{SO_4^{\bullet-}/MeOH} = 1.6 - 7.7 \times 10^7\ M^{-1}s^{-1}$, $k_{\bullet OH/MeOH} = 1.2 - 2.8 \times 10^9\ M^{-1}s^{-1}$,

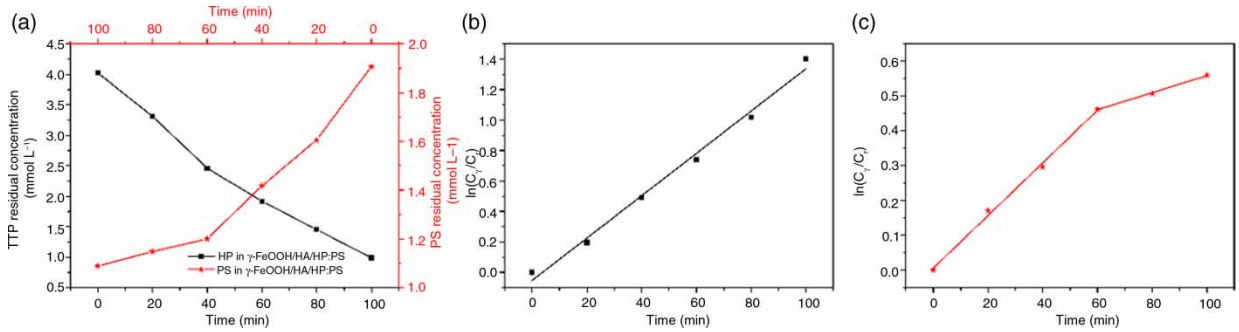

Figure 4 | (a) The HP and PS residual concentration; the HP (b) and PS (c) decomposition kinetics fitting curves.

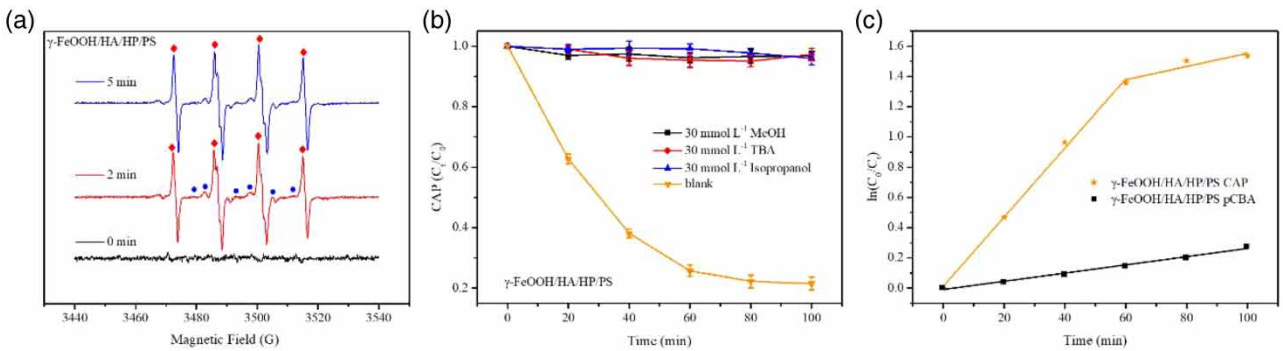

Figure 5 | (a) The EPR spectra; (b) The radical scavenging tests; (c) The kinetics curves of pCBA and CAP. ◆ represented the DMPO-OH adduct, • represented the DMPO-SO_4 adduct.

$k_{SO_4^{\bullet-}/TBA} = 4.0 - 9.1 \times 10^5\ M^{-1}s^{-1}$ and $k_{\bullet OH/TBA} = 3.8 - 7.6 \times 10^8\ M^{-1}s^{-1}$, respectively (Wang *et al.* 2017). The CAP degradation was completely suppressed by MeOH, TBA and Isopropanol, suggesting that •OH was the primary radical in the CAP degradation by γ-FeOOH/HA/HP/PS system (Hou *et al.* 2017).

The competition kinetic method was used to test the reaction rate constants of CAP with radicals at original pH by using pCBA as the competitor (Cao *et al.* 2020), as shown in Figure 5(c). According to our previous research, the $k_{\cdot OH,CAP}$ was $6.10 \times 10^9\ M^{-1}s^{-1}$ in γ-FeOOH/HA/HP system. The $k_{\cdot OH,CAP}$ was $4.24 \times 10^{10}\ M^{-1}s^{-1}$ in the initial phase (0–60 min) and $8.15 \times 10^9\ M^{-1}s^{-1}$ in the second phase (60–100 min) in γ-FeOOH/HA/HP/PS system, respectively. The rate was higher in the double oxidant system than in the single oxidant system. The result further confirmed the advantages of dual-oxidant system.

3.6. The role of hydroxylamine

The introduction of HA into HP/PS system could lead to a significant increase of the CAP removal efficiency. The degradation efficiency of CAP increased from 3.69% to 81.60% with HA concentration increasing from 0 mmol L^{-1} to 3 mmol L^{-1}, but the degradation efficiency decreased slightly when the HA concentration increased to 4 mmol L^{-1}, as shown in Figure 3(e). The HA accelerated the reduction of $\equiv Fe^{3+}$ to produce $\equiv Fe^{2+}$ for activating HP and PS. However, the competitive consumption of radicals with excess HA was the reason for the slight decrease of CAP degradation efficiency (Luo *et al.* 2021b). The dynamic fitting curves of CAP degradation under different HA dosage was shown in Figure 6(a). The whole reaction process was two-stage reaction kinetics. In the fast reaction stage, plenty of $\equiv Fe^{3+}$ was rapidly restored by HA, which caused the fast degradation of CAP. After HA was consumed, the generation of $\equiv Fe^{2+}$ was slow, the formation of reactive species was hindered, leading to a follow-up slow oxidation stage (Li *et al.* 2020).

The XPS spectra of γ-FeOOH before and after the catalytic reaction were favorable to evaluate the changes of Fe (Figure 6(b)) and O (Figure 6(c)) valence state in the HP/PS activation. The peaks at 711.61 eV and 725.21 eV belonged to the binding energy of $2p_{3/2}$ and $2p_{1/2}$ of $\equiv Fe^{3+}$ of γ-FeOOH. After degradation, the new peaks at 710.65 eV and 724.25 eV appeared which were $\equiv Fe^{2+}$ (Guo *et al.* 2019a; Wang *et al.* 2020). And $\equiv Fe^{3+}$ and $\equiv Fe^{2+}$ were 58.22% and 41.78% of the total iron surface atoms after reaction. This result suggested that the reduction of $\equiv Fe^{3+}$ to $\equiv Fe^{2+}$ occurred on the surface of γ-FeOOH. In addition, the O 1s peaks could be split into the lattice oxygen (O_{lat}, Fe-O-Fe and Fe-OH) at 530.03 eV and 531.20 eV, the surface adsorbed oxygen (O_{surf}) at 532.04 eV and the adsorbed molecular water (O_{ads}) at 533.50 eV with atomic ratio of 69.84%: 23.78%: 6.38% before the degradation (Baltrusaitis *et al.* 2007; Kim *et al.* 2021). After the degradation, the atomic ratio of O_{lat}, O_{surf} and O_{ads} was 45.71%: 37.35%: 16.95%, respectively. The ratio of O_{lat} reduced, the ratio of O_{surf} and O_{ads} increased. The increase in the proportion of O_{ads} might be attributed to more adsorbed molecular water on the surface of γ-FeOOH. The slight decrease in O_{lat} was attributed to the surface reduction from $\equiv Fe^{3+}$ to $\equiv Fe^{2+}$. If the leaching iron concentration was less than 3.92 mg L^{-1}, the process was heterogeneous catalysis (Chou *et al.* 2001). The leaching concentration of iron ion was 0.843 mg L^{-1} after 100 min in HP/PS system. All the results confirmed that the degradation process occurs on the γ-FeOOH surface.

The degradation intermediates were detected through LC-MS, and eleven degradation intermediates were observed, and the details are exhibited in Figure 7 and Fig. S2. The oxidation and dehydration of CAP leaded to produce P_1 (Chen *et al.* 2019). The center C connecting aromatic ring was attacked to produce P_2 and P_3. Simultaneously, the ring was opened to

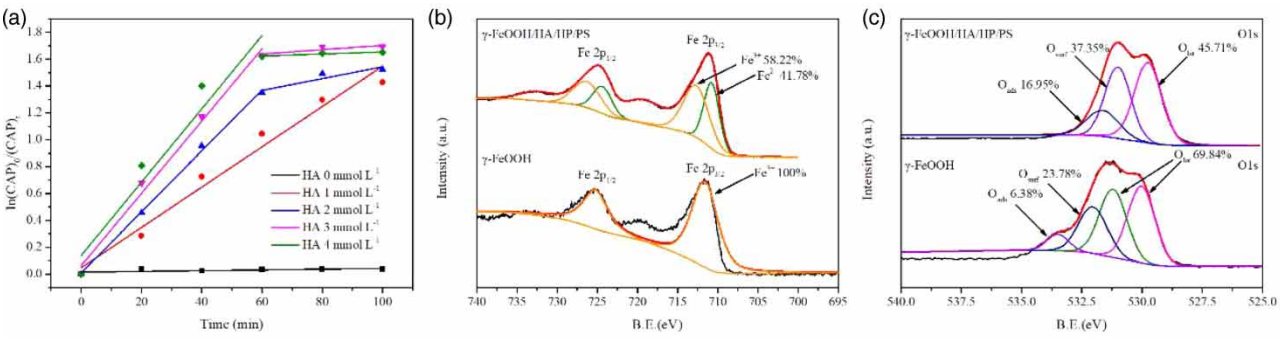

Figure 6 | (a) The kinetic fitting curves under different HA concentration; The XPS spectrum of (b) Fe2p and (c) O1s of γ-FeOOH before and after degradation.

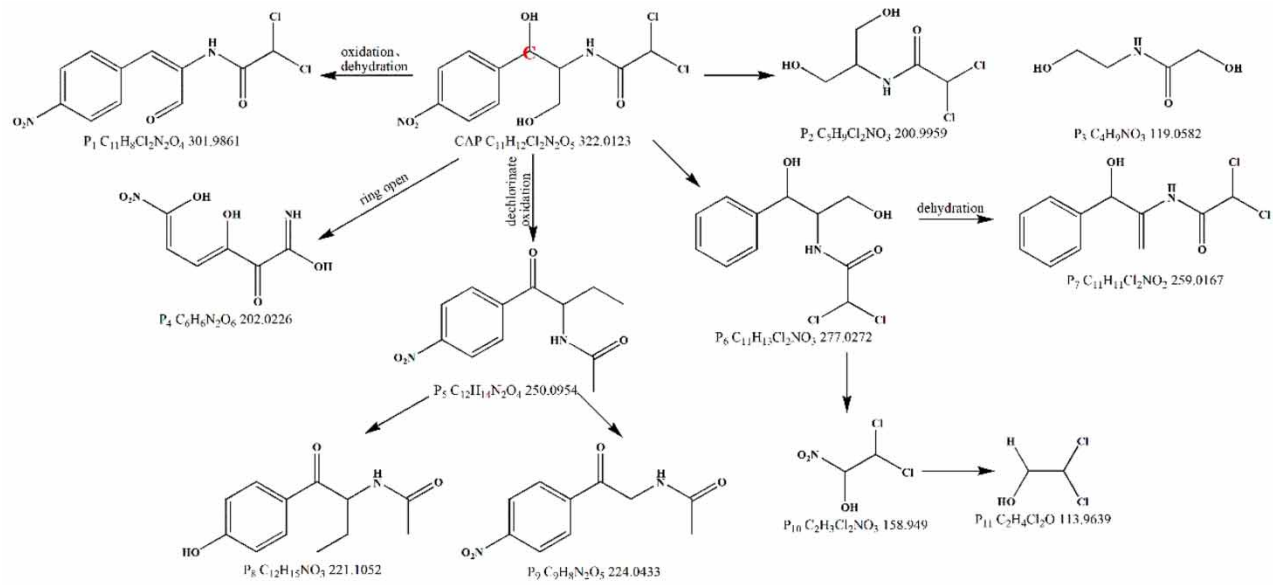

Figure 7 | The possible degradation products by γ-FeOOH/HA/HP/PS system.

form the intermediate P_4 (Yang *et al.* 2021). The radical attacked CAP by dechlorinate, dehydration and oxidation that result in the formation of P_5-P_7. The •OH attacked P_5 to generate the hydroxylated product P_8 (Guo *et al.* 2019b). A further attacking by radicals led to the the formation of P_9-P_{11}.

In brief, the CAP degradation process by γ-FeOOH could be depicted as follows. The HA restored the $\equiv Fe^{3+}$ into $\equiv Fe^{2+}$. The HP and PS interacted with $\equiv Fe^{2+}$ to produce highly oxidative radical species(•OH or $SO_4^{\bullet -}$). Then, these radical species attacked CAP and effectively transformed it into intermediates P_1-P_{11}.

4. CONCLUSIONS

In order to resource utilization of pipe deposits from water distribution networks, the primary composition of pipe deposits was employed as catalyst to active HP and PS to produce radicals for degradation pollutant. 92.05% PCE was oxidative degradation after 8 h. 73.31% CAP was removed in 100 min after the HA introduction. Furthermore, the reaction rate was HP/PS(0.0173 min^{-1}) > HP(0.0103 min^{-1}) > PS(0.0023 min^{-1}) and the reaction rate constant of radicals with CAP in HP/PS system was obvious higher. All the results implied that the dual-oxidant system has the unique advantages in pollutant removal. According to the result of XPS and ICP, the CAP degradation by HP/PS system was surface reaction. Eleven degradation intermediates were detected by LC-MS. The pipe deposits from water distribution networks has the capability to remove PCE and CAP in water. Although the effects of water quality and hydraulic conditions were not investigated, this study highlighted the advantage of HP/PS dual-oxidant system and the potential application of pipe deposits in water treatment in case of emerging contamination events.

ACKNOWLEDGEMENTS

This work was supported by the National Natural Science Foundation of China (No. 51778177) and Open Project of State Key Laboratory of Urban Water Resource and Environment, Harbin Institute of Technology (No. 2021TS10).

CONFLICTS OF INTEREST STATEMENT

The authors declare that they have no known competing financial interests or personal relationships that could have appeared to influence the work reported in this paper.

AUTHOR CONTRIBUTION

Dan Zhong: Resources, Funding acquisition; Fu He: Methodology, Investigation, Writing – original draft, Writing – review & editing; Wencheng Ma: Supervision; Yichuan Wu: The PCE degradation test; Jiaju Dong: Project administration.

DATA AVAILABILITY STATEMENT

All relevant data are included in the paper or its Supplementary Information.

REFERENCES

Antony, H., Legrand, L., Maréchal, L., Perrin, S., Dillmann, P. & Chaussé, A. 2005 Study of lepidocrocite γ-FeOOH electrochemical reduction in neutral and slightly alkaline solutions at 25 °C. *Electrochimica Acta* **51** (4), 745–753.

Baltrusaitis, J., Cwiertny, D. M. & Grassian, V. H. 2007 Adsorption of sulfur dioxide on hematite and goethite particle surfaces. *Physical Chemistry Chemical Physics* **9** (41), 5542–5554.

Cai, C., Zhang, Z., Liu, J., Shan, N., Zhang, H. & Dionysiou, D. D. 2016 Visible light-assisted heterogeneous Fenton with ZnFe2O4 for the degradation of Orange II in water. *Applied Catalysis B: Environmental* **182**, 456–468.

Cao, Y., Qiu, W., Zhao, Y., Li, J., Jiang, J., Yang, Y., Pang, S.-Y. & Liu, G. 2020 The degradation of chloramphenicol by O3/PMS and the impact of O3-based AOPs pre-oxidation on dichloroacetamide generation in post-chlorination. *Chemical Engineering Journal* **401**, 126146.

Chen, C., Liu, L., Guo, J., Zhou, L. & Lan, Y. 2019 Sulfur-doped copper-cobalt bimetallic oxides with abundant Cu(I): a novel peroxymonosulfate activator for chloramphenicol degradation. *Chemical Engineering Journal* **361**, 1304–1316.

Chen, W., Luo, Y., Ran, G. & Li, Q. 2020 Microwave-induced persulfate-hydrogen peroxide binary oxidant process for the treatment of dinitrodiazophenol industrial wastewater. *Chemical Engineering Journal* **382**, 122803.

Chou, S., Huang, C. & Huang, Y.-H. 2001 Heterogeneous and homogeneous catalytic oxidation by supported γ-FeOOH in a fluidized-bed reactor: kinetic approach. *Environmental Science & Technology* **35** (6), 1247–1251.

Cui, Y., Liu, S., Smith, K., Yu, K., Hu, H., Jiang, W. & Li, Y. 2016 Characterization of corrosion scale formed on stainless steel delivery pipe for reclaimed water treatment. *Water Research* **88**, 816–825.

Duan, X., Su, C., Zhou, L., Sun, H., Suvorova, A., Odedairo, T., Zhu, Z., Shao, Z. & Wang, S. 2016 Surface controlled generation of reactive radicals from persulfate by carbocatalysis on nanodiamonds. *Applied Catalysis B: Environmental* **194**, 7–15.

Epold, I., Trapido, M. & Dulova, N. 2015 Degradation of levofloxacin in aqueous solutions by Fenton, ferrous ion-activated persulfate and combined Fenton/persulfate systems. *Chemical Engineering Journal* **279**, 452–462.

Gao, Y., Wang, Q., Ji, G. & Li, A. 2022 Degradation of antibiotic pollutants by persulfate activated with various carbon materials. *Chemical Engineering Journal* **429**, 132387.

Gu, Z., Chen, W., Li, Q. & Zhang, A. 2019 Kinetics study of dinitrodiazophenol industrial wastewater treatment by a microwave-coupled ferrous-activated persulfate process. *Chemosphere* **215**, 82–91.

Guo, T., Wang, K., Zhang, G. & Wu, X. 2019a A novel α-Fe_2O_3@g-C3N4 catalyst: synthesis derived from Fe-based MOF and its superior photo-Fenton performance. *Applied Surface Science* **469**, 331–339.

Guo, H., Jiang, N., Wang, H., Lu, N., Shang, K., Li, J. & Wu, Y. 2019b Degradation of antibiotic chloramphenicol in water by pulsed discharge plasma combined with TiO_2/WO3 composites: mechanism and degradation pathway. *Journal of Hazardous Materials* **371**, 666–676.

He, D., Wu, X., Chen, Y., Situ, Y., Zhong, L. & Huang, H. 2018 In-situ growth of lepidocrocite on Bi_2O_3 rod: a perfect cycle coupling photocatalysis and heterogeneous fenton-like process by potential-level matching with advanced oxidation. *Chemosphere* **210**, 334–340.

He, F., Ma, W., Zhong, D. & Yuan, Y. 2020 Degradation of chloramphenicol by α-FeOOH-activated two different double-oxidant systems with hydroxylamine assistance. *Chemosphere* **250**, 126150.

Hou, X., Huang, X., Jia, F., Ai, Z., Zhao, J. & Zhang, L. 2017 Hydroxylamine promoted goethite surface Fenton degradation of organic pollutants. *Environmental Science & Technology* **51** (9), 5118–5126.

Huang, Z., Bao, H., Yao, Y., Lu, W. & Chen, W. 2014 Novel Green activation processes and mechanism of peroxymonosulfate based on supported cobalt phthalocyanine catalyst. *Applied Catalysis B: Environmental* **154–155**, 36–43.

Huang, W., Yuan, Y., Zhong, D., Ma, W., Yuan, Y. & Zhang, P. 2021 Adsorption and catalytic performance of pipe growth rings from water distribution networks using 5-BSA as the target pollutant. *Chemosphere* **284**, 131343.

Kim, B. G., Park, J., Choi, W., Han, D. S., Kim, J. & Park, H. 2021 Electrocatalytic arsenite oxidation using iron oxyhydroxide polymorphs (α-, β-, and γ-FeOOH) in aqueous bicarbonate solution. *Applied Catalysis B: Environmental* **283**, 119608.

Li, M., Yang, X., Wang, D. & Yuan, J. 2017 Enhanced oxidation of erythromycin by persulfate activated iron powder–H2O2 system: role of the surface Fe species and synergistic effect of hydroxyl and sulfate radicals. *Chemical Engineering Journal* **317**, 103–111.

Li, J., Xiao, C., Wang, K., Li, Y. & Zhang, G. 2019 Enhanced generation of reactive oxygen species under visible light irradiation by adjusting the exposed facet of FeWO4 nanosheets to activate oxalic acid for organic pollutant removal and Cr(VI) reduction. *Environmental Science & Technology* **53** (18), 11023–11030.

Li, Z.-Y., Wang, L., Liu, Y.-L., Zhao, Q. & Ma, J. 2020 Unraveling the interaction of hydroxylamine and Fe(III) in Fe(II)/Persulfate system: a kinetic and simulating study. *Water Research* **168**, 115093.

Liu, Y., Tan, N., Wang, B. & Liu, Y. 2019 Stepwise adsorption-oxidation removal of oxytetracycline by Zn0-CNTs-Fe3O4 from aqueous solution. *Chemical Engineering Journal* **375**, 121963.

Luo, H., Zeng, Y., He, D. & Pan, X. 2021a Application of iron-based materials in heterogeneous advanced oxidation processes for wastewater treatment: a review. *Chemical Engineering Journal* **407**, 127191.

Luo, H., Zeng, Y., Cheng, Y., He, D. & Pan, X. 2021b Activation of peroxymonosulfate by iron oxychloride with hydroxylamine for ciprofloxacin degradation and bacterial disinfection. *Science of The Total Environment* **799**, 149506.

Lyu, C., Zhang, L., He, D., Su, B. & Lyu, Y. 2021 Micrometer-sized NiOOH hierarchical spheres for enhanced degradation of sulfadiazine via synergistic adsorption and catalytic oxidation in peroxymonosulfate system. *Chinese Chemical Letters* **33** (2), 930–934.

Oliveira, C., Santos, M. S. F., Maldonado-Hódar, F. J., Schaule, G., Alves, A. & Madeira, L. M. 2012 Use of pipe deposits from water networks as novel catalysts in paraquat peroxidation. *Chemical Engineering Journal* **210**, 339–349.

Rao, Y. F., Qu, L., Yang, H. & Chu, W. 2014 Degradation of carbamazepine by Fe(II)-activated persulfate process. *Journal of Hazardous Materials* **268**, 23–32.

Rastogi, A., Al-Abed, S. R. & Dionysiou, D. D. 2009 Sulfate radical-based ferrous–peroxymonosulfate oxidative system for PCBs degradation in aqueous and sediment systems. *Applied Catalysis B: Environmental* **85** (3), 171–179.

Romero, A., Santos, A., Vicente, F. & González, C. 2010 Diuron abatement using activated persulphate: effect of pH, Fe(II) and oxidant dosage. *Chemical Engineering Journal* **162** (1), 257–265.

Shao, Y., Sun, Q., Wang, L., Zhan, W., Zhang, H. & Zhong, H. 2022 Migration and transformation of Sb are affected by Mn(III/IV) associated with lepidocrocite originating from Fe(II) oxidation. *Journal of Environmental Sciences* **115**, 308–318.

Shapiro, S. D., Busenberg, E., Focazio, M. J. & Plummer, L. N. 2004 Historical trends in occurrence and atmospheric inputs of halogenated volatile organic compounds in untreated ground water used as a source of drinking water. *Science of The Total Environment* **321** (1), 201–217.

Song, X., Tian, J., Shi, W., Cui, F. & Yuan, Y. 2020 Significant acceleration of Fe(2+)/ peroxydisulfate oxidation towards sulfisoxazole by addition of mos2. *Environmental Research* **188**, 109692.

Walters, E., McClellan, K. & Halden, R. U. 2010 Occurrence and loss over three years of 72 pharmaceuticals and personal care products from biosolids–soil mixtures in outdoor mesocosms. *Water Research* **44** (20), 6011–6020.

Wang, Q., Lu, X., Cao, Y., Ma, J., Jiang, J., Bai, X. & Hu, T. 2017 Degradation of Bisphenol S by heat activated persulfate: kinetics study, transformation pathways and influences of co-existing chemicals. *Chemical Engineering Journal* **328**, 236–245.

Wang, Z., Lai, C., Qin, L., Fu, Y., He, J., Huang, D., Li, B., Zhang, M., Liu, S., Li, L., Zhang, W., Yi, H., Liu, X. & Zhou, X. 2020 ZIF-8-modified $MnFe_2O_4$ with high crystallinity and superior photo-Fenton catalytic activity by Zn-O-Fe structure for TC degradation. *Chemical Engineering Journal* **392**, 124851.

Wu, D., Ye, P., Wang, M., Wei, Y., Li, X. & Xu, A. 2018 Cobalt nanoparticles encapsulated in nitrogen-rich carbon nanotubes as efficient catalysts for organic pollutants degradation via sulfite activation. *Journal of Hazardous Materials* **352**, 148–156.

Xu, X., Yang, Y., Jia, Y., Lian, X., Zhang, Y., Feng, F., Liu, Q., Xi, B. & Jiang, Y. 2019 Heterogeneous catalytic degradation of 2,4-dinitrotoluene by the combined persulfate and hydrogen peroxide activated by the as-synthesized Fe-Mn binary oxides. *Chemical Engineering Journal* **374**, 776–786.

Yan, N., Liu, F. & Huang, W. 2013 Interaction of oxidants in siderite catalyzed hydrogen peroxide and persulfate system using trichloroethylene as a target contaminant. *Chemical Engineering Journal* **219**, 149–154.

Yang, L.-X., Yang, J.-C. E. & Fu, M.-L. 2021 Magnetic $CoFe_2O_4$ nanocrystals derived from MIL-101 (Fe/Co) for peroxymonosulfate activation toward degradation of chloramphenicol. *Chemosphere* **272**, 129567.

Zhong, D., He, F., Ma, W., Yuan, Y. & Fang, T. 2019 Removal of tetrachloroethylene from aqueous media by means of adsorption or degradation of growth ring of water distribution network. *Journal of Environmental Engineering* **145** (11), 05019005.

Zhou, L., Shao, Y., Liu, J., Ye, Z., Zhang, H., Ma, J., Jia, Y., Gao, W. & Li, Y. 2014 Preparation and characterization of magnetic porous carbon microspheres for removal of methylene blue by a heterogeneous Fenton reaction. *ACS Appl Mater Interfaces* **6** (10), 7275–7285.

First received 9 November 2021; accepted in revised form 14 February 2022. Available online 28 February 2022